Achieving High Efficiency and Improved Stability in ITO-Free Transparent Organic Light-Emitting Diodes with Conductive Polymer Electrodes

Yong Hyun Kim, Jonghee Lee,* Simone Hofmann, Malte C. Gather, Lars Müller-Meskamp, and Karl Leo*

Efficient transparent organic light-emitting diodes (OLEDs) with improved stability based on conductive, transparent poly(3,4-ethylenedioxythiophene): poly(styrenesulfonate) (PEDOT:PSS) electrodes are reported. Based on optical simulations, the device structures are carefully optimized by tuning the thickness of doped transport layers and electrodes. As a result, the performance of PEDOT:PSS-based OLEDs reaches that of indium tin oxide (ITO)-based reference devices. The efficiency and the long-term stability of PEDOT:PSS-based OLEDs are significantly improved. The structure engineering demonstrated in this study greatly enhances the overall performances of ITO-free transparent OLEDs in terms of efficiency, lifetime, and transmittance. These results indicate that PEDOT:PSS-based OLEDs have a promising future for practical applications in low-cost and flexible device manufacturing.

1. Introduction

Organic light-emitting diodes (OLEDs) have attracted a great deal of attention as future lighting sources and in recent years they have already found application in commercial small display devices.[1,2] For realizing the full advantages of OLEDs, such as being transparent and flexible, the development of efficient electrodes is essential. The commonly used indium tin oxide (ITO) as a bottom electrode significantly increases device costs due to limited indium supply and the inherent brittleness of the material hinders the applications in flexible devices.[3,4] Therefore alternative electrodes such as silver nanowires,[5,6] carbon nanotubes,[7,8] thin metal films,[9,10] graphene layers,[11] and conductive polymers[12–14] are widely investigated to replace ITO. Poly(3,4-ethylenedioxythiophene):poly(styrenesurfonate) (PEDOT:PSS) is regarded as an especially promising alternative electrode due to its high conductivity and transmittance, flexibility, and low-cost.[15,16] It is reported that OLEDs as well as organic solar cells based on PEDOT:PSS electrodes have shown promising features.[12–14] In particular, as shown in our previous study, thin films of PEDOT:PSS optimized by a solvent post-treatment resulted in drastically improved electrical and stability properties, and allowed successful application in organic solar cells as an alternative electrode.[13,14] A major drawback of PEDOT:PSS films is their deposition from a water-based solution, which significantly deteriorates the performance of the organic devices in terms of efficiency as well as lifetime due to residual water in the finished product.[13,17–19] Therefore, one should pay a great attention not only to the efficiency of PEDOT:PSS-based devices but also to their stability and try to find a way to improve both of them.

Up to now, most studies of alternative electrodes have focused on achieving high device efficiency. The thickness of OLEDs is typically in the range of hundreds nanometers so out-coupled light is greatly influenced by light interference effects. Therefore, for any alternative electrode for OLEDs, the device structure has to be carefully optimized in terms of thin-film optical effects. Most importantly, since the performance of OLEDs is strongly modulated by the thicknesses of the different layers, each layer thickness needs to be optimized. As different electrodes have different optical properties, this process also needs to take into account the type of electrodes in order to achieve optimum out-coupling, i.e., constructive interference. Given this complexity of multi-layer OLED stacks, a full optical optimization of the device is required to compare stacks comprising different electrodes. Partial optimization might lead to inconclusive results, since the performance potential might be shadowed by poor optical optimization. So far, many studies do not consider this effect, i.e., they use identical device structures for reference and test devices. Moreover, for transparent OLEDs further optimization is required to control the ratio of top and bottom emission.[20–25]

Y. H. Kim, Dr. L. Müller-Meskamp, Prof. K. Leo
Dresdner Innovationszentrum für Energieeffizienz
Institut für Angewandte Photophysik
Technische Universität Dresden
01062 Dresden und Fraunhofer COMEDD
01109 Dresden, Germany
E-mail: yong.hyun.kim@iapp.de

Y. H. Kim, Dr. J. Lee, S. Hofmann, Prof. M. C. Gather,
Dr. L. Müller-Meskamp, Prof. K. Leo
Institut für Angewandte Photophysik
Technische Universität Dresden
01062 Dresden, Germany
E-mail: jonghee.lee@etri.re.kr

Dr. J. Lee
OLED Research Section
Electronics and Telecommunications Research Institute (ETRI)
Daejeon 305-700, Korea

DOI: 10.1002/adfm.201203449

Here, we demonstrate high performance ITO-free transparent OLEDs based on PEDOT:PSS electrodes. This is the first report, to our knowledge, to realize high efficiency together with long lifetime in the transparent OLEDs based on polymeric electrodes. The device performance is carefully optimized by tuning the thickness of the optical spacer layer and the PEDOT:PSS electrode. We find optimum device structures for different types of electrodes and thus demonstrate the great importance of electrode-specific stack engineering. The resulting PEDOT:PSS-based transparent OLEDs reach an external quantum efficiency (EQE) comparable to the ITO reference devices. Simulated values of photon flux obtained for these OLEDs using a numerical optical model are consistent with experimental optimization results. Moreover, the structure engineering leads to significantly improved long-term stability and transmittance of PEDOT:PSS-based devices. Considering the improved efficiency, lifetime, and transmittance of devices, the structure engineering proposed here can translate into a universal approach towards efficient and long-living ITO-free transparent OLEDs.

2. Results and Discussion

To figure out the effect of the device structure on the performance of OLEDs, different hole transport layer (HTL) and PEDOT:PSS thicknesses are investigated. Since the HTL thickness determines the position of the emission layer and emitting dipoles relative to the boundaries of the stack, controlling its thickness is crucial to obtain a maximum EQE. The overall device structure is illustrated in **Figure 1**a; the selected stacks are visualized in the simulated photon flux map in Figure 1b. The transmittance of 60 nm and 130 nm thick PEDOT:PSS films used in this work are 88.9% and 84.4% at a wavelength of 550 nm, respectively (Figure 1c). The transmittance of the ITO reference film (83.6%) is close to that of the 130 nm thick PEDOT:PSS film. Since the refractive indices and extinction coefficients of the two investigated electrode materials differ substantially (see Supporting Information), it is important that the device structure is modified to the respective optimum stacks according to the type of electrodes, using thin film optics. Although both 60 nm and 130 nm thick PEDOT:PSS thin films yield much higher sheet resistances of 209 ohm sq^{-1} and 93 ohm sq^{-1}, respectively, compared to ITO (30 ohm sq^{-1}), the following results show a promising performance of PEDOT:PSS-based OLEDs in small area devices. To scale-up of OLEDs based on PEDOT:PSS electrodes, an additional metal grid within the active area is required to reduce electrical losses. A simplified relationship between the transmittance and the sheet resistance in homogenous thin films can be derived from the following equation:[14,26]

$$T = \left(1 + \frac{Z_0}{2R_S}\frac{\sigma_{Op}}{\sigma_{dc}}\right)^{-2} \quad (1)$$

where T is the transmittance, R_S is the sheet resistance, Z_0 (377 ohm) is the impedance of free space, and σ_{Op} and σ_{dc} are the optical and dc conductivities, respectively. The value

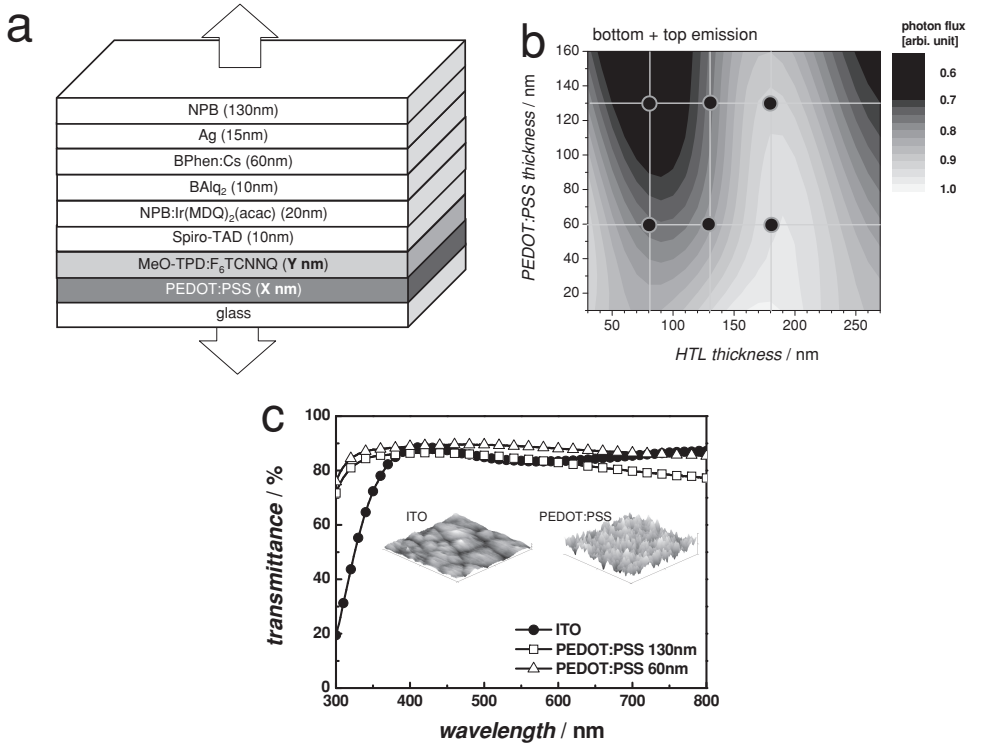

Figure 1. a) The device structure of ITO-free transparent red OLEDs based on a PEDOT:PSS electrode. The thicknesses of PEDOT:PSS and HTL are varied. (*X*: 60, 130 nm, *Y*: 80, 130, 180 nm). b) Simulated out-coupled photon flux in both bottom and top directions as a function of HTL and PEDOT:PSS thickness. Black dots represent the selected thicknesses for the fabrication of OLEDs. c) Transmittances of the electrodes used. The inset shows the surface topography of ITO and PEDOT:PSS, measured by AFM ($1 \times 1\ \mu m^2$).

of $\sigma_{dc}\sigma_{Op}^{-1}$ is frequently used as figure of merit for a transparent electrode. The calculated $\sigma_{dc}\sigma_{Op}^{-1}$ value of 60 nm and 130 nm thick PEDOT:PSS films are 52.2 and 46, respectively. Their $\sigma_{dc}\sigma_{Op}^{-1}$ values exceed the minimum $\sigma_{dc}\sigma_{Op}^{-1}$ ratio of 35, which is sometimes cited as a minimum requirement for practical use. Thus, the PEDOT:PSS films show great performance as highly conductive electrodes and maybe used in practical device applications.[26]

The surface morphology of the electrodes can greatly influence the shunt behavior of OLEDs in the low voltage regime. As shown in the inset of Figure 1c, the surface of ITO is very smooth whereas PEDOT:PSS shows a rough topography by comparison. The corresponding root-mean-square roughness values of ITO and PEDOT:PSS are around 0.4 nm and 1.6 nm, respectively. In the literature, thin films of PEDOT:PSS are frequently reported to smooth the ITO surface and reduce electrical shorts. The relatively high roughness of PEDOT:PSS used in our experiment, however, is due to the use of different, highly conductive formulation and it is further aggravated during the post-annealing process directly after spin-coating of films. During this process, the residual solvent, i.e., ethylene glycol, evaporates, which remarkably transforms the surface topography of the films. Despite the relatively rough surface of PEDOT:PSS, it can be successfully used in organic solar cells as well as in OLEDs.[12,14]

Prior to the fabrication of devices, we simulate the external photon flux of OLEDs in order to optimize the device structure as shown in Figure 1b. The simulation is based on a transfer matrix approach for obtaining the electromagnetic field in planar OLED structures.[27,28] The number of out-coupled photons is calculated according to

$$\text{photon flux} \propto \frac{2\pi}{hc}\int\int \lambda\, I'_e(\lambda,\ \theta)\sin\theta \mathrm{d}\lambda \mathrm{d}\theta \tag{2}$$

where λ is the wavelength, θ is the viewing angle, I'_e is the simulated spectral radiant intensity, h is the Planck constant, and c is the speed of light in vacuum. Exciton annihilation processes such as triplet-triplet annihilation and triplet-polaron annihilation are not considered in this simulation. Therefore, the comparison to experimentally obtained EQEs is performed in the low current density region, where annihilation processes are of minor importance. It is shown that the thicknesses of the bottom electrodes and the HTL significantly influence the photon flux. The maximum photon flux of PEDOT:PSS-based OLEDs is obtained for a ≈180 nm thick HTL and a rather thin PEDOT:PSS layer. The relatively large optical absorption coefficient of PEDOT:PSS is a limiting factor in the OLED performance; from an optical viewpoint a thin and highly transparent PEDOT:PSS is therefore desirable for high efficiency devices.

Based on the simulation predictions, six kinds of ITO-free OLEDs with various HTL and PEDOT:PSS thicknesses and three kinds of reference ITO-based OLEDs with various HTL thicknesses are fabricated. **Figure 2** presents the EQE data of those OLEDs. The EQE is calibrated using the angular dependent emission spectra, ensuring reasonable results. It is important that the EQE for transparent OLEDs needs to be

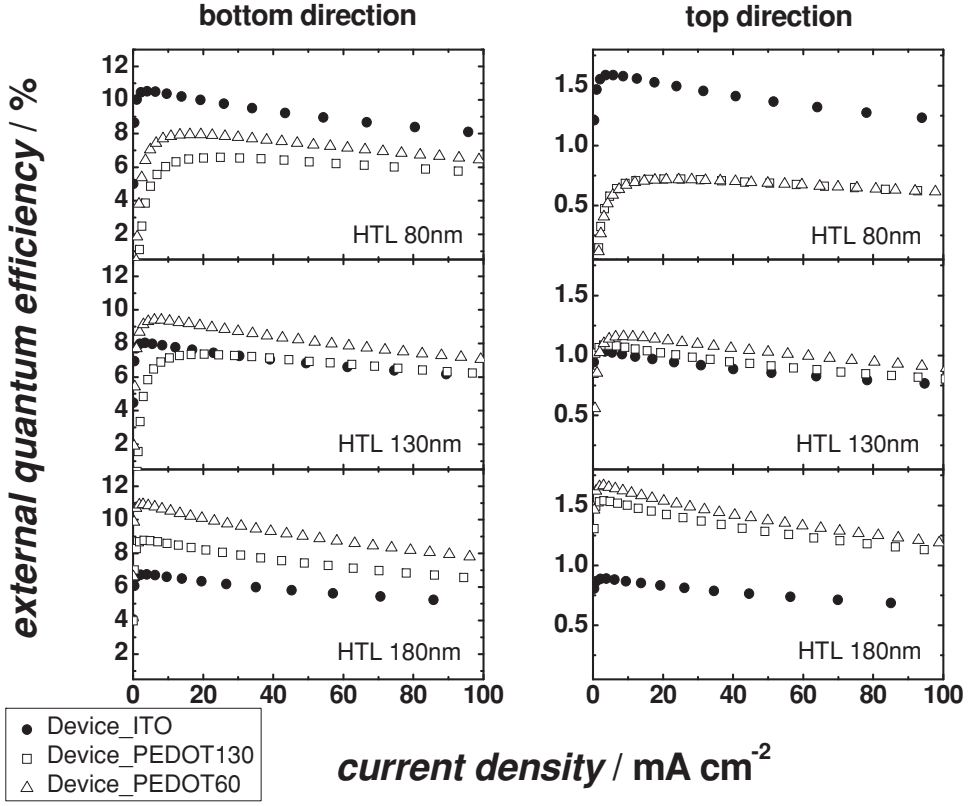

Figure 2. The EQE of ITO- and PEDOT:PSS-based OLEDs as a function of the type of electrodes and HTL thicknesses.

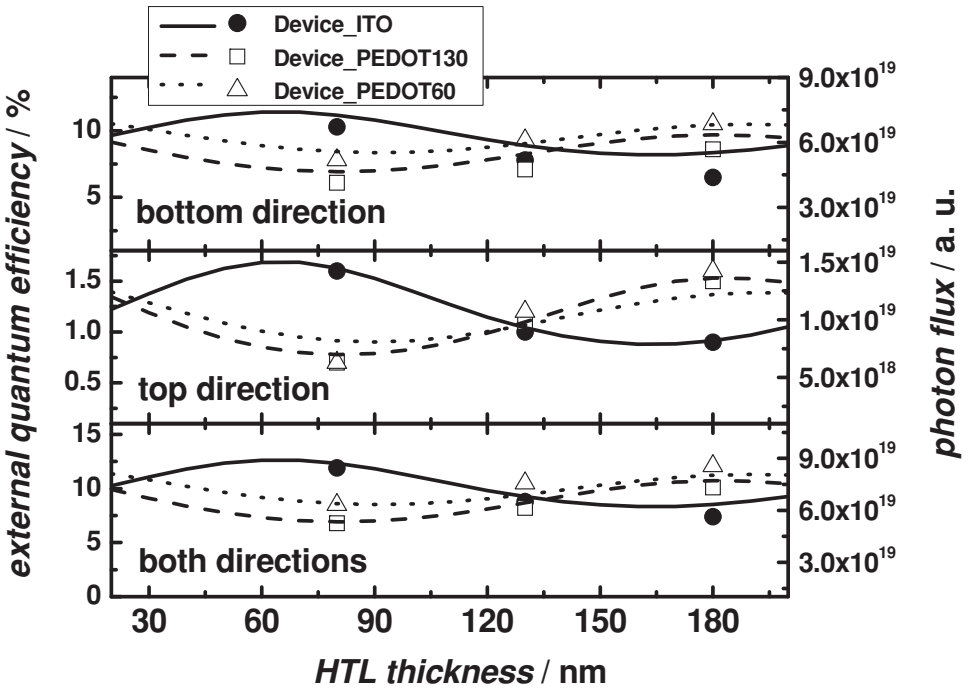

Figure 3. The comparison of EQEs and corresponding photon fluxes for bottom, top emission, and the sum of both, obtained from experiment (symbols) and optical simulation (lines), respectively.

evaluated taking the angular dependence behavior into account since the top emission significantly deviates from the Lambertian behavior.[22,29] The EQE is calculated by

$$\mathrm{EQE} = \frac{2\pi e}{Ihc}\int\int \lambda I_e(\lambda,\theta)\sin\theta \mathrm{d}\lambda \mathrm{d}\theta \quad (3)$$

where e is the elementary charge, I is the current through the device and I_e is the measured spectral radiant intensity. It is observed that the optimum HTL thicknesses are different for different kinds of bottom electrodes, seen from both simulation and experimental results. In the series of OLEDs with ITO (Device_ITO) bottom contacts, the highest EQE of 11.9% (sum of bottom and top emission at a current density of 10 mA cm^{-2}) is observed at a HTL thickness of 80 nm. For the PEDOT:PSS-based devices, the OLEDs having a 60 nm thick PEDOT:PSS (Device_ PEDOT60) electrode exhibit the highest EQE of 12.1% at a HTL thickness of 180 nm. Despite the higher sheet resistance of PEDOT:PSS compared to ITO, the performance of PEDOT:PSS-based OLEDs in optimal condition is comparable to that of ITO-based OLEDs. The high performance of PEDOT:PSS-based OLEDs is mainly attributed to the weak microcavity effect, which reduces organic waveguided mode as described by Cai et al.[30] The lower refractive index of PEDOT:PSS ($n \approx 1.5$), which nearly matches to glass ($n \approx 1.5$), causes a different cavity length and organic waveguided mode from those of ITO-based OLEDs. In addition, the use of a doped HTL allows an ohmic interface between PEDOT:PSS and HTL despite the high sheet resistance of PEDOT:PSS, which enhances hole injection and minimizes energy loss.[13,31] This is observed experimentally, as the onset voltages of the PEDOT:PSS- and ITO-based OLEDs in our work are almost equal (2.3 V), despite of the work function difference between PEDOT:PSS (≈5.0 eV) and ITO (≈4.8 eV).

As expected, the device performance is significantly changed by the various HTL thicknesses. **Figure 3** shows both experimental EQE and simulated photon fluxes, which are agree well. The EQE of the Device_ITO decreases with increasing HTL thickness for both bottom and top emission. In contrast, devices with PEDOT:PSS electrodes show an increasing EQE with increasing HTL thickness. Furthermore, the thickness of the PEDOT:PSS electrodes remarkably affects the performance of the OLEDs. The Device_ PEDOT60 series consistently shows higher EQEs than devices with 130 nm thick PEDOT:PSS electrodes (Device_ PEDOT130). This is seen for all HTL thicknesses studied here and in both bottom and top emission. These results indicate that thickness tuning for both doped transport layers and electrodes is of great importance to maximize the amount of light extracted from the devices. It should be highlighted that the OLED performance is drastically influenced by the device geometry, especially the type of electrodes. Photon flux for the Device_ITO reaches its maximum at the same HTL thickness where PEDOT:PSS-based OLEDs have a minimum. Thus, to study the application of alternative electrodes in OLEDs, the adequate device structure needs to be investigated taking the changed optics of the respective electrodes into account. As expected, the behavior of the current efficiency in OLEDs is similar to that of EQE (see Supporting Information). Furthermore, it is observed that the bottom to top emission ratio can be also controlled by changing the thickness of the HTL or the electrodes as shown in **Table 1**.

Figure 4a shows the normalized electroluminescence (EL) spectra of the Device_ITO and Device_PEDOT60 at HTL

Table 1. EQE values and bottom to top EQE ratio of OLEDs with various electrode types and HTL thicknesses at a driving current density of 10 mA cm^{-2}.

		Device_ITO	Device_PEDOT130	Device_PEDOT60
HTL 80 nm	bottom	10.3%	6.1%	7.8%
	top	1.6%	0.7%	0.7%
	total	**11.9%**	**6.8%**	**8.5%**
	bottom:top	6.4:1	8.7:1	11.1
HTL 130 nm	bottom	7.8%	7.1%	9.3%
	top	1.0%	1.1%	1.2%
	total	**8.8%**	**8.2%**	**10.5%**
	bottom:top	7.8:1	6.5:1	7.8:1
HTL 180 nm	bottom	6.5%	8.6%	10.5%
	top	0.9%	1.5%	1.6%
	total	**7.4%**	**10.1%**	**12.1%**
	bottom:top	7.2:1	5.7:1	6.6:1

thicknesses of 80 nm and 180 nm, respectively, i.e., at the thickness for which each device shows the best EQE value. The normalized EL spectra of the best performing ITO- and PEDOT:PSS-based OLEDs are nearly equal for both bottom and top emissions with the peak at a wavelength of 617 nm. However, non-optimized devices show blue shifted EL peaks together with reduced EQE, due to the device stack deviating from the optimal condition. Spectral angular-dependent emission characteristics are also investigated for the best devices in each series of ITO- and PEDOT:PSS-based OLEDs by spectrogoniometer measurements, showing the influence of different electrodes on the emission distribution with viewing angles (Figure 4b). The bottom emission of both devices is closer to the Lambertian emission pattern than the top emission which shows the non-Lambertian nature. Especially, the Device_PEDOT60 exhibits a nearly perfect Lambertian emission pattern in the bottom direction due to the optimized cavity length.

For practical applications of hygroscopic PEDOT:PSS electrodes in OLEDs, realizing a long and stable lifetime of the devices is of great importance. To investigate the effect of the device structure on the lifetime of the devices, the Device_PEDOT60 with a HTL thickness of 80 nm and the Device_PEDOT130 with a HTL thickness of 80 nm are chosen for lifetime measurements (**Figure 5**). At high luminance of around 1500 cd m^{-2}, which is much brighter than in display applications (400–500 cd m^{-2}), both PEDOT:PSS-based OLEDs do not exhibit any drop of luminance over 900 h, showing very stable performance. This indicates that water induced degradation from hygroscopic PEDOT:PSS electrodes is not a significant issue at this condition. To accelerate aging further, we increase the initial luminance to around 5000 cd m^{-2}. In contrast to the test at lower luminance, the devices with higher luminance exhibit clear degradation behavior. The luminance of the Device_ PEDOT130 exponentially decreases while the Device_PEDOT60 shows a linear drop of luminescence. It is clearly shown that the thinner PEDOT:PSS electrode leads to better device stability. Our previous study showed that PEDOT:PSS thin films having a lower amount of PSS yielded better chemical stability due to less water uptake.[14] The amount of residual

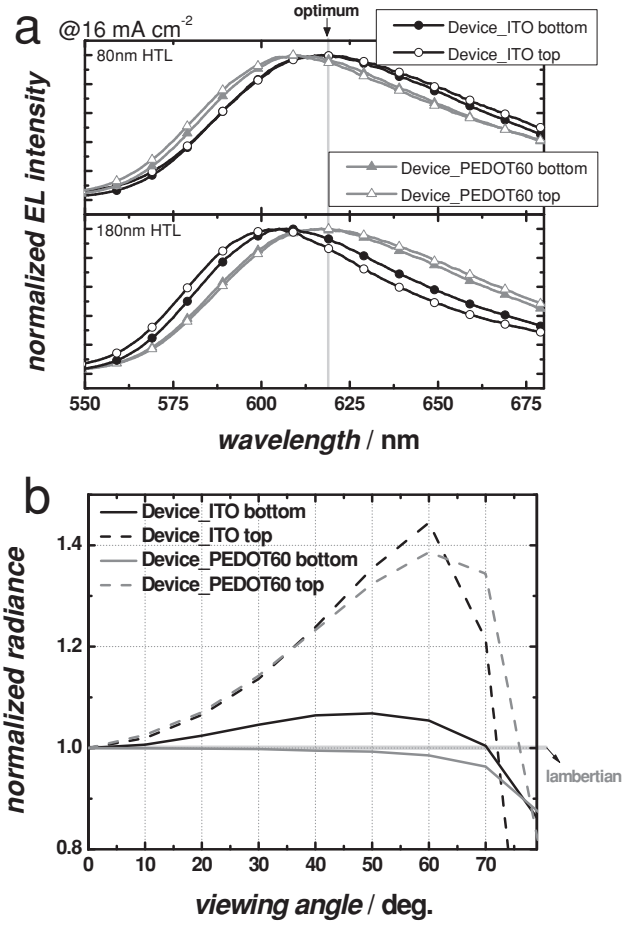

Figure 4. a) The normalized electroluminescence spectra of Device_ITO and Device_PEDOT:PSS60 with 80 nm and 180 nm thick HTLs, respectively. b) The normalized radiance of devices.

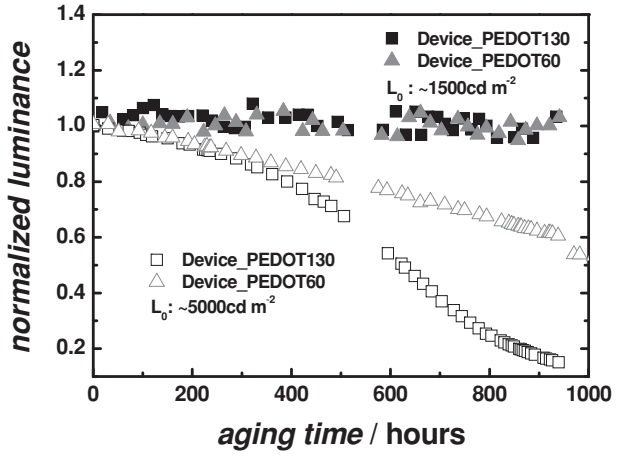

Figure 5. Aging characteristics of PEDOT:PSS-based OLEDs having a different electrode thickness. The encapsulated devices are aged over around 900 hours with an initial luminance of around 1500 cd m^{-2} or 5000 cd m^{-2}. Constant currents are applied for each sample according to the corresponding luminance.

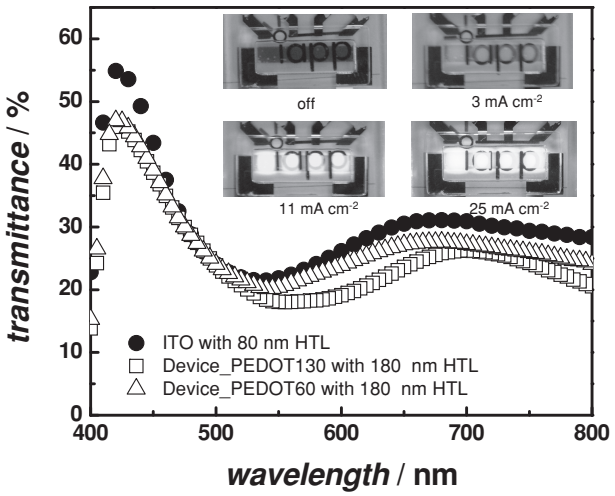

Figure 6. Transmittances of transparent OLEDs with respect to different bottom electrodes. Inset shows the top view of red emitting light of PEDOT:PSS-based OLEDs with different applied current densities. Four pixels are connected for lighting.

water inside the PEDOT:PSS layer strongly depends on the amount of PSS contained, due to the hygroscopic nature of PSS.[13,14,17–19] Thus, thicker PEDOT:PSS electrodes result in poorer stability of the device. It is, therefore, expected that the optimization of the PEDOT:PSS electrode thickness is crucial for designing stable OLEDs.

Figure 6 shows the transmittance spectra and photographs of selected ITO-free transparent OLEDs. As can be seen from the photographs, the PEDOT:PSS-based OLEDs show good transmittances in the off-state as well as on-state. The average transmittances in the visible range of the Device_ITO and the PEDOT:PSS-based OLEDs series are 25–28% and 22–25%, respectively. Due to negligible optical losses in the HTL, the HTL thickness can be increased further without affecting the transmittance of the OLEDs. The thinner Device_PEDOT60 series shows 2–3% higher transmittances than the Device_PEDOT130 series at the same HTL thickness regime, indicating that the thickness and absorption of PEDOT:PSS are the critical parameters determining the transmittance of devices. According to the structure engineering, thinner PEDOT:PSS electrodes are more beneficial for transparent OLEDs in our study in terms of efficiency, lifetime, and transmittance of devices.

3. Conclusions

In summary, we demonstrate efficient ITO-free transparent OLEDs with conductive polymer electrodes. The high performance of the OLEDs is achieved by careful optimization of the device stack, supported by optical simulation, which fits well with the experimental results. The PEDOT:PSS-based OLEDs achieve comparable performance to the ITO-based OLEDs. We highlight the importance of structure engineering according to the type of electrodes, which should be addressed for achieving maximum potential. The doping technology used for the HTL leads to a very low onset voltage of the PEDOT:PSS-based OLEDs despite of the high sheet resistance of electrode. Moreover, a reasonably long lifetime of the PEDOT:PSS-based OLEDs is obtained by tuning the electrode thickness. The structure engineering performed in this work, which improves efficiency, stability, and transmittance of OLEDs with a polymer electrode, is beneficial for realizing low-cost, flexible, and long living OLEDs applications. We believe that this study can provide a comprehensive guide to achieving high efficiency, stable PEDOT:PSS-based transparent OLEDs and important contributions to take laboratory OLED research to commercial production.

4. Experimental Section

Fabrication and Characterization of PEDOT:PSS Electrodes: PEDOT:PSS (Clevios PH1000, Heraeus, Germany) mixed with 6 vol% of ethylene glycol was spun onto glass substrates at 1000 rpm and 2500 rpm for 30 s. The thicknesses of resulting films were around 130 nm and 60 nm, respectively. Spin-coated films were subsequently annealed on a hot plate at 120 °C for 15 min in ambient. The sheet resistance of films was measured by a four point probe setup with a source measurement unit (Keithley 2400). The thickness of the films was examined by a surface profilometer (Veeco Dektak 150). Transmittance was obtained by a spectrophotometer (Perkin Elmer Lambda 900). The atomic force microscopy (AFM) images were taken in tapping mode (AIST-NT Combiscope).

Fabrication and Characterization of OLEDs: For removal of residual water in the PEDOT:PSS electrode, the prepared PEDOT:PSS films were thermally annealed at 110 °C for 30 min in a vacuum chamber directly before evaporation of organic materials. Small molecule layers were thermally evaporated onto the bottom electrodes in a high vacuum chamber (K. J. Lesker, U. K.) at a base pressure of around 10^{-8} mbar using shadow masks. The layer sequence for devices was as follows (bottom to top): ITO or PEDOT:PSS/*X* nm (*N*,*N*,*N*′,*N*′-tetrakis(4-methoxyphenyl)-benzidine) (MeO-TPD):2,2′-(perfluoronaphthalene-2,6-diylidene)dimalononitrile (F_6TCNNQ) (4wt%)/10nm 2,2′,7,7′-tetrakis-(*N*,*N*′-diphenylamino)-9,9′-spirobifluorene (Spiro-TAD)/20 nm *N*,*N*′-di(naphthalene-1-yl)*N*,*N*′-diphenyl-benzidine (NPB):iridium(III)bis(2-methyldibenzo-[f,h]chinoxalin)(acetylacetonat) ($Ir(MDQ)_2(acac)$) (10 wt%)/10 nm bis(2-methyl-8-chinolinolato)-4-(phenyl-phenolato)-aluminum-(III) ($Balq_2$)/60 nm 4,7-diphenyl-1,10-phenanthroline (BPhen):Cs (1:1)/15 nm Ag/130 nm NPB. The device structure is visualized in Figure 1a. After evaporation, all devices were encapsulated with cover glass using epoxy glue without getter material. The active areas of the devices are ≈6.1 mm^2, measured using an optical microscope. Current-voltage-luminance characteristics and electroluminescence spectra were examined using an automated source-measure unit system (Keithley SM2400) and a calibrated spectrometer (CAS140CT-153, Instrument Systems GmbH). External quantum efficiencies were calibrated with the spatial emission of the devices, carried out by a spectrogoniometer. Emission characteristics of devices were obtained at angles θ from 0° to 90° in 10° steps.

Supporting Information

Supporting Information is available from the Wiley Online Library or from the author.

Acknowledgements

The authors thank O. R. Hild and C. May at Fraunhofer COMEDD for supporting the DIZEeff. This work was funded by the European Union (EFRE), the Fraunhofer Gesellschaft, and the Free State of Saxony as part of the Dresdner Innovationszentrum Energieeffizienz. J.L. acknowledges

the Alexander von Humboldt Foundation and the IT R&D program of MKE/KEIT (Grant No. 10041416, The core technology development of light and space adaptable new mode display for energy saving on 7 inch and 2 W).

Received: November 22, 2012
Revised: January 4, 2013
Published online: February 26, 2013

[1] M. Baldo, D. O'Brien, Y. You, A. Shoustikov, S. Sibley, M. Thompson, S. Forrest, *Nature* **1998**, *395*, 151.
[2] S. Reineke, F. Lindner, G. Schwartz, N. Seidler, K. Walzer, B. Lüssem, K. Leo, *Nature* **2009**, *459*, 234.
[3] Z. Chen, B. Cotterell, W. Wang, E. Guenther, S. J. Chua, *Thin Solid Films* **2001**, *394*, 201.
[4] S. R. Forrest, *Nature* **2004**, *428*, 911.
[5] J. Y. Lee, S. T. Connor, Y. Cui, P. Peumans, *Nano Lett.* **2008**, *8*, 689.
[6] Z. Yu, Q. Zhang, L. Li, Q. Chen, X. Niu, J. Liu, Q. Pei, *Adv. Mater.* **2011**, *23*, 664.
[7] J. Li, L. Hu, L. Wang, Y. Zhou, G. Grüner, T. J. Marks, *Nano Lett.* **2006**, *6*, 2472.
[8] D. Zhang, K. Ryu, X. Liu, E. Polikarpov, J. Ly, M. E. Tompson, C. Zhou, *Nano Lett.* **2006**, *6*, 1880.
[9] J. Meiss, M. Riede, K. Leo, *Appl. Phys. Lett.* **2009**, *94*, 013303.
[10] L. Smith, J. Wasey, W. L. Barnes, *Appl. Phys. Lett.* **2004**, *84*, 2986.
[11] J. Wu, M. Agrawal, H. A. Becerril, Z. Bao, Z. Liu, Y. Chen, P. Peumans, *ACS Nano* **2009**, *4*, 43.
[12] K. Fehse, K. Walzer, K. Leo, W. Lövenich, A. Elschner, *Adv. Mater.* **2007**, *19*, 441.
[13] Y. H. Kim, C. Sachse, M. Hermenau, K. Fehse, M. Riede, L. Müller-Meskamp, K. Leo, *Appl. Phys. Lett.* **2011**, *99*, 113305.
[14] Y. H. Kim, C. Sachse, M. L. Machala, C. May, L. Müller-Meskamp, K. Leo, *Adv. Funct. Mater.* **2011**, *21*, 1076.
[15] L. Groenendaal, F. Jonas, D. Freitag, H. Pielartzik, J. R. Reynolds, *Adv. Mater.* **2000**, *12*, 481.
[16] S. Kirchmeyer, K. Reuter, *J. Mater. Chem.* **2005**, *15*, 2077.
[17] A. Nardes, M. Kemerink, M. De Kok, E. Vinken, K. Maturova, R. Janssen, *Org. Electron.* **2008**, *9*, 727.
[18] K. Fehse, R. Meerheim, K. Walzer, K. Leo, W. Lövenich, A. Elschner, *Appl. Phys. Lett.* **2008**, *93*, 083303.
[19] M. Jørgensen, K. Norrman, F. C. Krebs, *Sol. Energy Mater. Sol. Cells* **2008**, *92*, 686.
[20] G. Gu, V. Bulović, P. Burrows, S. Forrest, M. Thompson, *Appl. Phys. Lett.* **1996**, *68*, 2606.
[21] S. Ju, J. Li, J. Liu, P. C. Chen, Y. Ha, F. Ishikawa, H. Chang, C. Zhou, A. Facchetti, D. B. Janes, *Nano Lett.* **2007**, *8*, 997.
[22] J. Lee, S. Hofmann, M. Furno, M. Thomschke, Y. H. Kim, B. Lüssem, K. Leo, *Org. Electron.* **2011**, *12*, 1383.
[23] J. Meyer, T. Winkler, S. Hamwi, S. Schmale, H. H. Johannes, T. Weimann, P. Hinze, W. Kowalsky, T. Riedl, *Adv. Mater.* **2008**, *20*, 3839.
[24] M. Pfeiffer, S. Forrest, X. Zhou, K. Leo, *Org. Electron.* **2003**, *4*, 21.
[25] J. Lee, S. Hofmann, M. Thomschke, M. Furno, Y. H. Kim, B. Lüssem, K. Leo, *Appl. Phys. Lett.* **2011**, *99*, 073303.
[26] V. Scardaci, R. Coull, J. N. Coleman, *Appl. Phys. Lett.* **2010**, *97*, 023114.
[27] M. Furno, R. Meerheim, M. Thomschke, S. Hofmann, B. Lüssem, K. Leo, *Proc. SPIE* **2010**, *7617*, 761716.
[28] R. Meerheim, M. Furno, S. Hofmann, B. Lüssem, K. Leo, *Appl. Phys. Lett.* **2010**, *97*, 253305.
[29] S. Hofmann, M. Thomschke, P. Freitag, M. Furno, B. Lüssem, K. Leo, *Appl. Phys. Lett.* **2010**, *97*, 253308.
[30] M. Cai, Z. Ye, T. Xiao, R. Liu, Y. Chen, R. W. Mayer, R. Biswas, K. M. Ho, R. Shinar, J. Shinar, *Adv. Mater.* **2012**, *24*, 4337.
[31] J. Blochwitz, T. Fritz, M. Pfeiffer, K. Leo, D. Alloway, P. Lee, N. Armstrong, *Org. Electron.* **2001**, *2*, 97.